Reverse Epitaxy of Ge: Ordered and Faceted Surface Patterns

Xin Ou,[1] Adrian Keller,[1] Manfred Helm,[1,2] Jürgen Fassbender,[1,2] and Stefan Facsko[1,*]

[1]*Institute of Ion Beam Physics and Materials Research, Helmholtz-Zentrum Dresden-Rossendorf, Bautzner Landstrasse 400, 01328 Dresden, Germany*

[2]*Technische Universität Dresden, 01062 Dresden, Germany*

(Received 21 March 2013; published 3 July 2013)

Normal incidence ion irradiation at elevated temperatures, when amorphization is prevented, induces novel nanoscale patterns of crystalline structures on elemental semiconductors by a reverse epitaxial growth mechanism: on Ge surfaces irradiation at temperatures above the recrystallization temperature of 250 °C leads to self-organized patterns of inverse pyramids. Checkerboard patterns with fourfold symmetry evolve on the Ge (100) surface, whereas on the Ge (111) surface, isotropic patterns with a sixfold symmetry emerge. After high-fluence irradiations, these patterns exhibit well-developed facets. A deterministic nonlinear continuum equation accounting for the effective surface currents due to an Ehrlich-Schwoebel barrier for diffusing vacancies reproduces remarkably well our experimental observations.

DOI: 10.1103/PhysRevLett.111.016101 PACS numbers: 68.35.Ct, 79.20.Rf, 81.16.Rf, 81.65.Cf

Self-organized pattern formation in systems far from equilibrium is a fundamentally interesting phenomenon governed by the interplay of kinetic and diffusive mechanisms. In addition, surface patterns with nanoscale dimensions are of technological interest for applications in sublithographic surface templating and for quantum dot device fabrication [1]. They may be generated on surfaces by homoepitaxy [2,3], heteroepitaxy [4] or by energetic ion irradiation [5–7]. However, semiconductor surfaces become amorphous during ion irradiation at room temperature. At these conditions periodic ripple patterns oriented perpendicular or parallel to the ion beam direction and isotropic, hexagonally ordered, dot or hole patterns, independent of the crystal structure [8], have been observed [7]. The origin of these patterns is attributed to an interplay of surface instability due to sputtering and mass redistribution together with surface relaxation mechanisms [9,10]. At near normal incidence smoothing dominates on amorphized elemental materials [11]. On the other hand, metal surfaces remain crystalline during ion irradiation at room temperature [6]. They exhibit a much higher complexity of pattern formation due to additional instabilities resulting from anisotropies in surface diffusion and due to biased diffusion across step edges [12]. Similarities with homoepitaxy have been identified: layer by layer erosion has been observed on metals [13] as well as on semiconductor surfaces [14]. Furthermore, similar to mound formation in epitaxy, pit formation has been observed on ion irradiated metal surfaces [15,16]. Although the formation of pits has also been seen in low-fluence irradiations of semiconductors [17–19], dense and ordered patterns of faceted nanostructures, as found in homoepitaxy and heteroepitaxy, have not been observed until now on ion irradiated semiconductor surfaces.

In this letter we present the formation of regular patterns of crystalline structures induced by normal incidence ion irradiation of an elemental semiconductor, Ge, at elevated temperatures. Above the recrystallization temperature of 250 °C ion-induced bulk defects are dynamically annealed and the surface remains crystalline. By only increasing the irradiation temperature, instead of inducing surface smoothing, novel checkerboard patterns with crystalline facets appear exhibiting the symmetry of the surface. They strongly resemble mound patterns in homoepitaxial growth [2], but are reversed. The mechanism can thus be interpreted as reverse epitaxy. In analogy with the Villain instability in homoepitaxy resulting from the Ehrlich-Schwoebel (ES) barrier for an adatom descending a monoatomic step [20,21] we conclude that the formation of ion-induced crystalline patterns results from the existence of an ES barrier for the ascending of surface vacancies created by sputtering. Based on the proposed atomistic mechanisms we derived a continuum equation which describes remarkably well the experimentally observed surface evolution.

Samples cut from epi-ready Ge (100) wafers were irradiated by a broad 1 keV Ar^+ ion beam at normal incidence without any pre-treatment. The irradiations were performed in a high vacuum chamber with a Kaufman ion source. The samples were heated by a boron nitride heater from the backside. The surface topography was analyzed after irradiations *ex situ* by atomic force microscopy (AFM).

In Fig. 1 AFM images of Ge (100) surfaces irradiated with ion fluences of 3×10^{18} cm^{-2} and different surface temperatures ranging from 230 °C to 430 °C are shown. At temperatures below 250 °C the Ge surface remains smooth after irradiation [Fig. 1(a)]. At these conditions the Ge surface is amorphized by ion irradiation and smoothing by surface diffusion and mass redistribution dominates [11]. The initial roughness of the virgin Ge surface of 0.7 nm is reduced to 0.18 nm. At temperatures higher than 250 °C checkerboard patterns appear after irradiation indicating that an additional ion-induced instability appears. The structures of the pattern have a rectangular

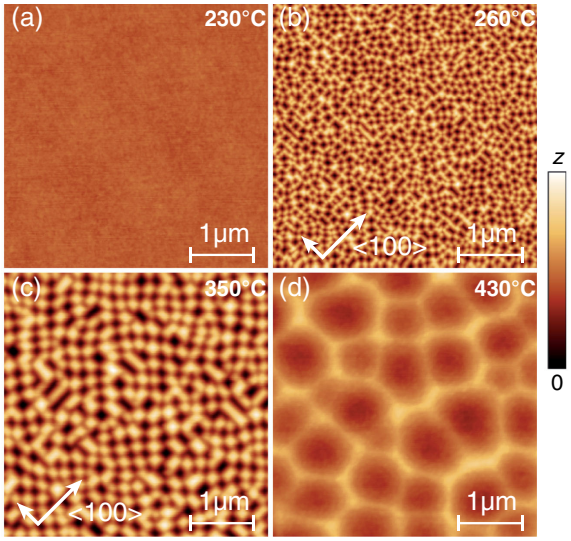

FIG. 1 (color online). AFM height images of Ge (100) surfaces after ion irradiation with an ion fluence of 3×10^{18} cm^{-2} at temperatures of 230 °C, 260 °C, 350 °C, and 430 °C. The ⟨100⟩ crystal directions are marked by arrows. (a) $z = 8$ nm; (b) $z = 38$ nm; (c) $z = 38$ nm; (d) $z = 8$ nm.

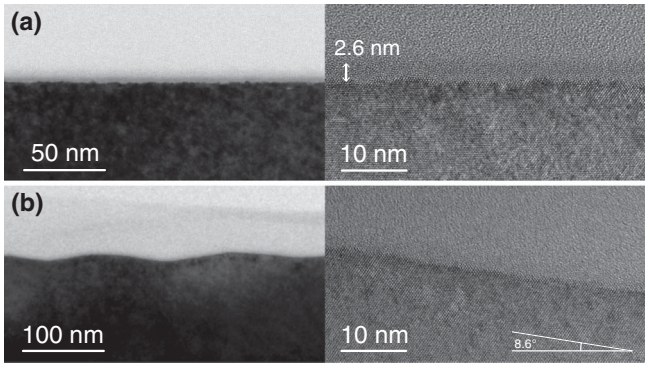

FIG. 2. TEM images of Ge surfaces in cross section irradiated at temperatures of (a) 230 °C and (b) 260 °C. In (a) a 2.6 nm thick amorphous layer can be identified, whereas in (b) no amorphous layer is visible. In Fig. 2(b) right the angle of the facet is shown with the horizontal line parallel to the (100) surface.

shape and an average size of ≈150 nm with an orientation in the ⟨100⟩ direction [Fig. 1(b)]. The structures size increases with irradiation temperature as a checkerboard pattern with an average size of ≈260 nm develops at 350 °C [Fig. 1(c)]. At 430 °C the structure size increases further while the symmetry is changed to an isotropic pattern of pits with diameter of 300–1000 nm. The order is much lower and the structure size distribution much broader than for the checkerboard patterns. Finally, at temperatures above 500 °C the surface is again smoothed by ion irradiation, similar to irradiations at 230 °C (not shown).

We investigated the microstructure of the patterns in cross section with transmission electron microscopy (TEM). In Fig. 2 TEM images of Ge (100) surfaces are shown, which were irradiated at temperatures of 230 °C and 260 °C, respectively. At 230 °C the surface is flat and a 2.6 nm thick amorphous Ge layer is visible. At 260 °C and higher no amorphous layer is visible. In the TEM image of the Ge surfaces irradiated at 260 °C facets are visible. In the following we use the term "facet" in a more general sense as a surface region with a predominant azimuthal and polar orientation. The facets are not atomically flat but exhibit a roughness on the nanoscale, a few Å high, induced by the stochastic nature of sputtering. The angle between the facets and the (100) plane is determined to 8°–10°.

The transition from smoothing to roughening by ion irradiation between 230 °C and 260 °C can be attributed to the temperature at which amorphization by ion irradiation is prevented. Ion-induced vacancies and interstitials in the bulk are dynamically annealed above this temperature and only adatoms and surface vacancies remain as defects. At these temperatures we also expect that Ar is not incorporated into the crystal and diffuses out without influencing the surface kinetics. Hence, surface patterns result from the kinetics of adatoms and vacancies created by the incident ion beam; however, vacancy kinetics is expected to dominate because more vacancies are created by sputtering. In analogy to the ES barrier for adatoms, i.e., the diffusion barrier for an adatom to descent a step edge, a barrier exists for a vacancy to ascend into the next higher terrace. Thus, vacancies are trapped on lower terraces leading to reverse growth of surface structures, i.e., the formation of pyramidal pits. At higher temperature the mobility of vacancies increases and the nucleation density decreases leading to pits with larger separation and size. If the thermal energy of vacancies is high enough to overcome the ES barrier, the surface will remain smooth as experimentally observed for temperatures above 430 °C.

The evolution of crystalline surfaces is described by atomistic processes on terraces, steps, and kinks [22]. Diffusion and attachment of adatoms and vacancies at steps and kinks is expected to be anisotropic. The pyramidal pits on Ge (100) exhibit facets oriented along the ⟨100⟩ crystal direction. The emergence of these edges is attributed to an additional barrier at kink sites, similar to the barrier at step edges [23]. On the (100) surface the kink ES barrier is responsible for the repulsion of vacancies on the fast diffusing ⟨110⟩ step edges. This mechanism has also been proposed for the formation of mounds oriented in the ⟨100⟩ directions in homoepitaxy of Ge (100) [24]. The energy barrier for the diffusion around corners is expected to be smaller than for crossing step edges. Therefore, the kink ES barrier vanishes already at temperatures where the terrace ES barrier is still active and isotropic pit patterns should appear. This is indeed observed for irradiations at 430 °C [Fig. 1(d)] where the square symmetry of the pattern disappears and dense round pits are formed.

In order to further elucidate the formation mechanism we investigated the roughening and coarsening behavior of the checkerboard pattern on Ge (100) at 350 °C. Figure 3(a) shows the evolution of Ge(100) surface as well as the corresponding two-dimensional fast Fourier transform

(FFT) and two-dimensional angle distribution [25] as a function of ion fluence. The FFT reveals the symmetry and the order of the pattern, whereas from the two-dimensional angle distribution the formation of predominant facets can be deduced. After irradiations with a fluence of 1×10^{17} cm^{-2} a pit pattern with no clear orientation is visible. The angle distribution is isotropic with a maximum at 0°. At higher fluence of 1×10^{18} cm^{-2} the pattern already exhibits an orientation along the ⟨100⟩ crystal direction. The angle distribution reveals a fourfold symmetry with broad maxima around 9.5°. Finally, at 1×10^{19} cm^{-2} the angle distribution has four distinct narrow peaks around 11°. The peaks in the angle distribution are a clear signature for facet formation on the patterned Ge (100) surface. The azimuthal and polar orientation of the facets are close to the {106} (9.5°) and {105} (11.3°) crystal planes. The formation of these facets results from the instability due to biased diffusion of vacancies created by ion irradiation, whereas the angle of the facets is determined by kinetic or energetic stabilization of low index planes under the given kinetic restrictions. Such low index planes are observed in Ge homoepitaxy [2,3,26] and heteroepitaxy on Si [1,27,28]. The energy minimization of the {106} or {105} planes results from the effective reduction of dangling bonds by dimerization on the (100) terraces. On Si and Ge the (105) surface is found to be atomically rough [28] and flat (105) facets are only observed in strained Ge "hut" islands. However, we expect that under ion irradiation the stabilized low index planes are metastable, like the (100) surface, and the facet angle will increase further. In our experiments we did not observe saturation of the facet angle up to ion irradiation fluences of 1×10^{19} cm^{-2}.

For the description of the temporal evolution of the surface during ion irradiation a continuum equation is derived considering sputtering and mass distribution by the incident ion beam [9,10,29,30] and surface diffusion of ion induced vacancies on crystalline surfaces [31]. The temporal evolution of the surface height, $h(x, y, t)$, is described by a deterministic partial differential equation [32],

$$\frac{\partial h}{\partial t} = -v_0 - \nu \nabla^2 h - \nabla \boldsymbol{j}_{\mathrm{ion}} - \nabla \boldsymbol{j}_{\mathrm{diff}}, \qquad (1)$$

with v_0 the constant erosion rate of the flat Ge surface, $\nu \nabla^2 h$ the curvature dependent sputter rate [9], $\boldsymbol{j}_{\mathrm{ion}}$ the surface current resulting from the ballistic mass redistribution [10,33], and $\boldsymbol{j}_{\mathrm{diff}}$ surface currents due to diffusion [20]. Mass redistribution by ion impact is proportional to the surface curvature, $\nabla^2 h$, like the curvature dependent sputtering rate, however, with a positive coefficient for incidence angles smaller than 45° [10]. At normal and small incidence angles this stabilizing mechanism overcompensates the destabilizing sputtering term, $\nu \nabla^2 h$,

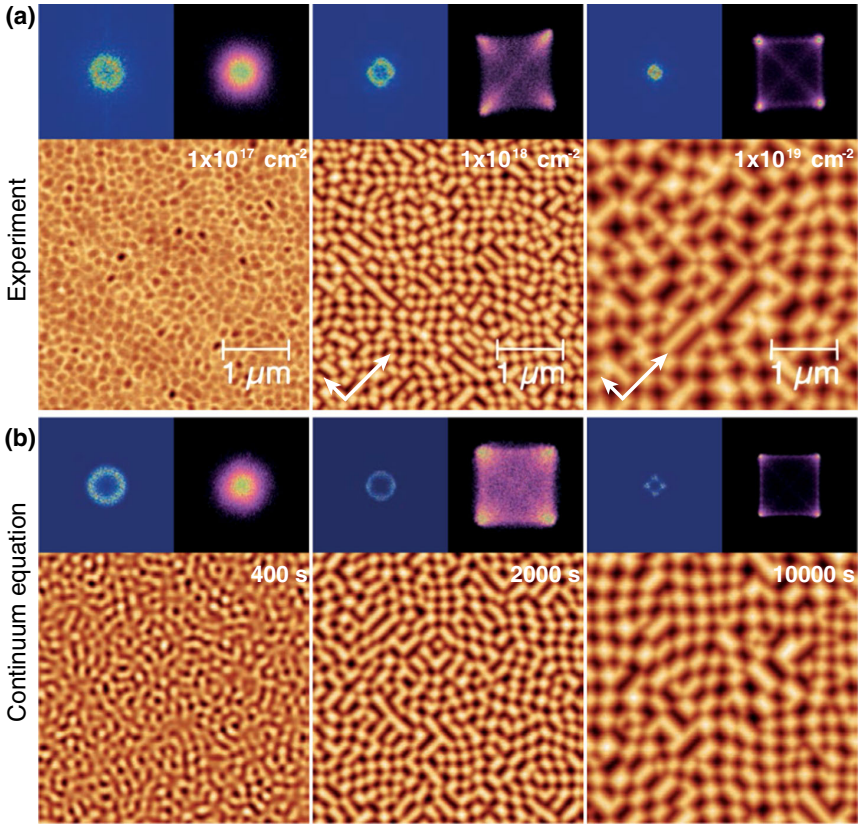

FIG. 3 (color online). (a) AFM images of Ge (100) surfaces irradiated at 350 °C and fluences of 1×10^{17} cm^{-2}, 1×10^{18} cm^{-2}, and 1×10^{19} cm^{-2}. (b) Snapshots of the numerical integration of the continuum equation with $\epsilon = 1$, $\kappa = 4$, $\sigma = -1$, and $\delta = 25$. Above the images the two-dimensional FFT (left) and the two-dimensional angle distribution (right) are shown.

and the amorphous surface is effectively smoothed at these conditions. The pattern formation on crystalline surfaces results from an additional kinetic instability due to the ES barrier. As shown later, this instability is included in the diffusive current, $\boldsymbol{j}_{\mathrm{diff}}$, and also proportional to the surface curvature with a negative coefficient. Thus, ion induced mass redistribution and sputtering can only reduce the ES instability and pattern formation is dominated by the biased diffusive surface currents. For the strong erosive regime this is a quite surprising result explaining the strong resemblance of ion induced patterns with patterns observed in homoepitaxy [2].

On amorphous surfaces, diffusion is described by the isotropic Herring-Mullins (HM) surface diffusion [34]. On crystalline surfaces, the diffusive current has to include atomistic surface currents on terraces, across terrace steps, along steps, and across kinks [35]. On the crystalline Ge (100) surface an isotropic surface diffusion has to be assumed as well described by the HM surface diffusion current, $\boldsymbol{j}_{\mathrm{HM}}$, whereas diffusion across steps is biased by the ES barrier for ascending vacancies, resulting in a net uphill mass current, $\boldsymbol{j}_{\mathrm{ES}}$. The symmetry of the crystalline Ge(100) surface is taken into account by an anisotropic current vector, $\boldsymbol{j}_{ES}(\boldsymbol{m})$, which is a function of the surface slopes, $m_{(x,y)} = \partial_{(x,y)} h$ [36],

$$\boldsymbol{j}_{\mathrm{diff}} = \kappa\nabla(\nabla^2 h) + \sigma\nabla(\nabla h)^2 + \epsilon\begin{bmatrix} m_x(1-\delta m_x^2) \\ m_y(1-\delta m_y^2) \end{bmatrix}. \quad (2)$$

Here, the first term is the isotropic HM surface diffusion. The second term is called the ''conserved Kadar-Parisi-Zhang'' term and has been introduced as a nonlinear current corresponding to the ''nonconserved'' nonlinearity in the Kadar-Parisi-Zhang equation $(\lambda/2(\nabla h)^2)$ [20]. This nonlinear current is known to break the up or down symmetry, which is prominently seen in the high temperature round pit patterns [Fig. 1(d)] [37]. Finally, the third term describes the anisotropic ES surface current, $\boldsymbol{j}_{\mathrm{ES}}$ [38], which is pointing uphill for positive ϵ inducing a surface instability [20]. The anisotropy of this current has its origin in the anisotropy of the ES barrier itself as well as in additional currents due to step edge diffusion [39,40]. This kind of surface current leads to the formation of facets at angles for which the current becomes zero [31,35]. Close to these points the surface current is negative (positive) for smaller (larger) angles, leading to an increase (decrease) of the slope. The parameter δ determines the angle of the facets: $\theta = \pm\arctan(\sqrt{1/\delta})$. In the continuum equation the facet angle will saturate at the given zeros of the ES surface current. So in order to describe the experimentally observed surface dynamics a higher polynomial of the surface current has to be assumed with zeros at angles for every kinetically or thermodynamically stabilized facet.

In Fig. 3(b) snapshots of the numerical integration of the continuum equation and their corresponding two-dimensional FFTs and two-dimensional angle distribution are shown [41]. After 40 000 integration steps an isotropic pattern forms exhibiting a characteristic periodicity without facets. At 200 000 integration steps facets are already fully developed. The two-dimensional angle distribution reveals distinct peaks at 11° in diagonal direction of the simulation grid. The two-dimensional FFT shows a circular region already with a slight anisotropy along the k_x and k_y axes. Finally, at 1 000 000 steps, very sharp peaks appear in the two-dimensional angle distribution at positions expected from the zeros of the ES surface current. The two-dimensional FFT now also exhibits peaks corresponding to the fourfold symmetry of the pattern. The comparison with the experiments reveals a remarkable agreement. Furthermore, the proposed continuum equation is able to describe the different temperature regimes identified in Fig. 1 by choosing proper coefficients [42].

From the experimental fluence series in Fig. 3, we determined the temporal evolution of the surface topography. In Fig. 4 the roughness and the characteristic length of the pattern, determined from the first minimum in the height-height correlation functions [43], are shown as a function of ion fluence. A power law fit to the roughness reveals a growth exponent $\beta = 0.59 \pm 0.06$, which is close to the theoretical value of 0.5 for the so- called statistical growth limit corresponding to growth by random deposition [35]. However, due to the existence of an instability, larger exponents can be expected [44]. Furthermore, the pattern coarsens; i.e., the characteristic length increases with fluence. A power law fit reveals a coarsening exponent $1/z = 0.14 \pm 0.02$. Such small exponents have also been observed for mound coarsening in homoepitaxy [16]. Theoretically, a coarsening exponent of $1/4$ is predicted for an infinite ES barrier [23]. Smaller exponents are expected for moderate barriers in step edge diffusion [23]. The numerical integration of the continuum equation gives a growth exponent of $\beta = 0.45$ and a coarsening exponent of $1/z = 0.20$, in fair agreement with the experiments.

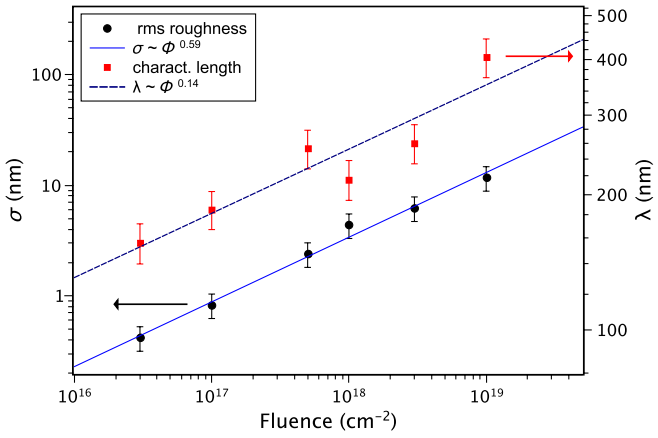

FIG. 4 (color online). Roughness and characteristic length of surface patterns on Ge(100) as a function of ion fluence. The lines represent power law fits to the data. The fluence Φ is given by ion flux times irradiation time.

Pattern formation by reverse epitaxy is a universal mechanism and can be achieved on many different crystalline materials. We identified the temperature window where patterns of crystalline structures are formed; i.e., the irradiation temperature is (i) above the dynamic recrystallization temperature of the material and (ii) low enough to establish an active ES barrier. At these conditions an excess of vacancies is created which are partially reflected at terrace steps inducing an effective uphill mass current. This instability leads to the formation of periodic patterns of inverse pyramids oriented along the crystalline directions of the surface. The faceting of the pyramids results from anisotropic surface currents due to a kink ES barrier. We could thus demonstrate that ion irradiation can induce patterns of faceted crystalline structures by a reverse epitaxy process. Therefore, this technique could establish as a complementary epitaxial method for the fabrication of high-quality crystalline semiconductor nanostructures.

The authors would like to acknowledge TEM analysis by Arndt Mücklich, fruitful discussions with Karl-Heinz Heinig, Jörg Grenzer, and Wolfhard Möller, and funding from the Deutsche Forschungsgemeinschaft (FOR845).

*s.facsko@hzdr.de

[1] C. Teichert, Phys. Rep. **365**, 335 (2002).
[2] J. E. Van Nostrand, S. J. Chey, M.-A. Hasan, D. G. Cahill, and J. E. Greene, Phys. Rev. Lett. **74**, 1127 (1995).
[3] J. Van Nostrand, S. Chey, and D. Cahill, Phys. Rev. B **57**, 12 536 (1998).
[4] J. Tersoff and R. M. Tromp, Phys. Rev. Lett. **70**, 2782 (1993).
[5] S. Facsko, T. Dekorsy, C. Koerdt, C. Trappe, H. Kurz, A. Vogt, and H. L. Hartnagel, Science **285**, 1551 (1999).
[6] U. Valbusa, C. Boragno, and F. B. de Mongeot, J. Phys. Condens. Matter **14**, 8153 (2002).
[7] W. L. Chan and E. Chason, J. Appl. Phys. **101**, 121301 (2007).
[8] S. Facsko, T. Bobek, H. Kurz, T. Dekorsy, S. Kyrsta, and R. Cremer, Appl. Phys. Lett. **80**, 130 (2002).
[9] R. M. Bradley and J. M. E. Harper, J. Vac. Sci. Technol. A **6**, 2390 (1988).
[10] B. Davidovitch, M. J. Aziz, and M. P. Brenner, Phys. Rev. B **76**, 205420 (2007).
[11] C. S. Madi, E. Anzenberg, K. F. Ludwig, and M. J. Aziz, Phys. Rev. Lett. **106**, 066101 (2011).
[12] S. Rusponi, G. Costantini, C. Boragno, and U. Valbusa, Phys. Rev. Lett. **81**, 2735 (1998).
[13] B. Poelsema, L. K. Verheij, and G. Comsa, Phys. Rev. Lett. **53**, 2500 (1984).
[14] P. Bedrossian, J. E. Houston, J. Y. Tsao, E. Chason, and S. T. Picraux, Phys. Rev. Lett. **67**, 124 (1991).
[15] T. Michely and G. Comsa, Surf. Sci. **256**, 217 (1991).
[16] J. A. Stroscio, D. T. Pierce, M. D. Stiles, A. Zangwill, and L. M. Sander, Phys. Rev. Lett. **75**, 4246 (1995).
[17] S. J. Chey, J. E. VanNostrand, and D. G. Cahill, Phys. Rev. B **52**, 16 696 (1995).
[18] J. Kim, D. G. Cahill, and R. S. Averback, Phys. Rev. B **67**, 045404 (2003).
[19] H. J. W. Zandvliet and E. de Groot, Surf. Sci. **371**, 79 (1997).
[20] J. Villain, J. Phys. I **1**, 19 (1991).
[21] J. G. Amar and F. Family, Phys. Rev. Lett. **77**, 4584 (1996).
[22] Z. Y. Zhang and M. G. Lagally, Science **276**, 377 (1997).
[23] J. G. Amar, Phys. Rev. B **60**, R11317 (1999).
[24] B. Shin, J. P. Leonard, J. W. McCamy, and M. J. Aziz, Appl. Phys. Lett. **87**, 181916 (2005).
[25] The two dimensional angle distribution is a histogram of pairs of angles in x and y direction with respect to the surface calculated by the surface gradients, $\partial h/\partial x$ and $\partial h/\partial y$, in x and y direction, respectively.
[26] J. E. Van Nostrand, S. J. Chey, and D. G. Cahill, J. Vac. Sci. Technol. B **13**, 1816 (1995).
[27] Y. W. Mo, D. E. Savage, B. S. Swartzentruber, and M. G. Lagally, Phys. Rev. Lett. **65**, 1020 (1990).
[28] M. Tomitori, K. Watanabe, M. Kobayashi, F. Iwawaki, and O. Nishikawa, Surf. Sci. **301**, 214 (1994).
[29] A. L. Barabási and H. E. Stanley, *Fractal Concepts in Surface Growth* (Cambridge University Press, Cambridge, England, 1995).
[30] S. Facsko, T. Bobek, A. Stahl, H. Kurz, and T. Dekorsy, Phys. Rev. B **69**, 153412 (2004).
[31] M. Siegert, Phys. Rev. Lett. **81**, 5481 (1998).
[32] Redistribution and diffusion processes are mass conserving and can therefore be described by surface currents.
[33] M. Moseler, P. Gumbsch, C. Casiraghi, A. C. Ferrari, and J. Robertson, Science **309**, 1545 (2005).
[34] W. W. Mullins, J. Appl. Phys. **30**, 77 (1959).
[35] T. Michely and J. Krug, *Islands, Mounds, and Atoms*, Springer Series in Surface Science Vol. 42, edited by G. Ertl, H. Lüth, and D. L. Mills, Patterns and Processes in Crystal Growth Far from Equilibrium (Springer Verlag, Berlin, Heidelberg, New York, 2004).
[36] M. Siegert and M. Plischke, Phys. Rev. Lett. **73**, 1517 (1994).
[37] For positive values of σ the surface evolves to patterns with mound structures, whereas for negative values of σ patterns of pit structures appear.
[38] The anisotropic ES surface current $\boldsymbol{j}_{\mathrm{ES}}$ has been introduced with an explicit term coupling the currents in x- and y-direction [31]; however, these terms are implicitly already contained in $\nabla \boldsymbol{j}_{\mathrm{ES}}$ and were therefore omitted for convenience.
[39] M. V. Ramana Murty and B. Cooper, Phys. Rev. Lett. **83**, 352 (1999).
[40] P. Politi and J. Krug, Surf. Sci. **446**, 89 (2000).
[41] See Supplemental Material at http://link.aps.org/supplemental/10.1103/PhysRevLett.111.016101 for details of the numerical integrations.
[42] See Supplemental Material at http://link.aps.org/supplemental/10.1103/PhysRevLett.111.016101 for numerical integrations at different temperatures and movies of the height evolution with different coefficients for the low- and high-temperature case.
[43] Y. Zhao, G.-C. Wang, and T.-M. Lu, *Characterization of Amorphous and Crystalline Rough Surface: Principles and Applications*, Experimental Methods in the Physical Sciences Vol. 37 (Academic Press, San Diego, 2001).
[44] R. Cuerno, H. A. Makse, S. Tomassone, S. T. Harrington, and H. E. Stanley, Phys. Rev. Lett. **75**, 4464 (1995).